

Optical Signatures of Defect Centres in Transition Metal Dichalcogenide Monolayers

Pedro Miguel M. C. de Melo* Zeila Zanolli* Matthieu J. Verstraete

Dr. Pedro Miguel Monteiro Campos de Melo nanomat/Q-mat/CESAM, Université de Liège, Institut de Physique, B-4000 Sart Tilman, Liège, Belgium

Chemistry Department, Debye Institute for Nanomaterials Science, Condensed Matter and Interfaces, Utrecht University, PO Box 80.000, 3508 TA Utrecht, The Netherlands

European Theoretical Spectroscopy Facility (ETSF) www.etsf.eu

Email: p.m.monteirocamposdemelo@uu.nl

Prof. Dr. Zeila Zanolli

Catalan Institute of Nanoscience and Nanotechnology (ICN2), CSIC and BIST, Campus UAB, Bellaterra, 08193 Barcelona, Spain

Chemistry Department, Debye Institute for Nanomaterials Science, Condensed Matter and Interfaces, Utrecht University, PO Box 80.000, 3508 TA Utrecht, The Netherlands

European Theoretical Spectroscopy Facility (ETSF) www.etsf.eu

Email: z.zanolli@uu.nl Prof. Dr. Matthieu Jean Verstraete

nanomat/Q-mat/CESAM, Université de Liège, Institut de Physique, B-4000 Sart Tilman, Liège, Belgium

European Theoretical Spectroscopy Facility (ETSF) www.etsf.eu

Keywords: *Optical absorption, Transition metal dichalcogenides, defect centres, quantum dots*

Even the best quality 2D materials have non-negligible concentrations of vacancies and impurities. It is critical to understand and quantify how defects change intrinsic properties, and use this knowledge to generate functionality. This challenge can be addressed by employing many-body perturbation theory to obtain the optical absorption spectra of defected transition metal dichalcogenides. Herein metal vacancies, which are largely unreported, show a larger set of polarized excitons than chalcogenide vacancies, introducing localized excitons in the sub-optical-gap region, whose wave functions and spectra make them good candidates as quantum emitters. Despite the strong interaction with substitutional defects, the spin texture and pristine exciton energies are preserved, enabling grafting and patterning in optical detectors, as the full optical-gap region remains available. A redistribution of excitonic weight between the A and B excitons is visible in both cases and may allow the quantification of the defect concentration. This work establishes excitonic signatures to characterize defects in 2D materials and highlights vacancies as qubit candidates for quantum computing.

Transition metal dichalcogenides (TMDs) have become strong contenders for the engineering of optical devices, especially thanks to their coupling of the spin and valley degrees of freedom, and the presence of strongly bound excitons, opening avenues for next generation opto-electronics^[1,2]. Manufactured samples have strongly improved in quality, but will always contain a significant concentration of defects^[3,4]. Graphene can be crystallized almost perfectly in very large flakes, but TMDs present many more natural defects, in particular chalcogen vacancies (see e.g. Ref.^[5]). On the bright side, defects and substitutional dopants can be used to tune the electronic structure and optical properties of materials^[6]. By doing so, devices sensitive to specific wavelengths and polarizations can be engineered (reviewed in Ref.^[7]), and can even behave as single photon emitters^[8]. There is an ongoing search for long lived spin states at room temperatures in TMDs. Here defects are expected to play a crucial role in both scattering and storing spin information - we showed recently that intrinsic scattering mechanisms (the electron-phonon interaction) can quickly destroy the pumped spin-polarisation^[9]. Chalcogen vacancies can also be used as grafting sites for functional groups, to create bio and chemical sensors^[10,11]. Alkane and other functional groups can be incorporated directly into the matrix (as opposed to thiol links, for instance, which necessitate Au). Carbon atoms have also been used as acceptor dopants for bulk semiconductors^[12]. In TMDs, mixed phases with transition metal carbides have been shown to have applications in catalysis^[13,14], while in MoS₂ it was shown that carbon substitutions had a strong effect on the TMD electronic and optical properties^[15,16].

Many experiments give access to the presence and properties of localized defects. In TMDs the most commonly used are: Scanning Tunnelling Microscopy which shows contrast changes due to chemical substitution and electron cloud reconstruction around defects^[17]; Scanning Tunnelling Spectroscopy, which

arXiv:2010.10222v2 [cond-mat.other] 21 Oct 2020

probes the detailed electronic structure at the defect site^[17]; optical spectroscopy showing absorption and photoluminescence by the defect-induced states^[18–20]; tunnelling transport from insulated contacts through a core material, which is resonant through defect states in the core band gap^[19]; transmission electron microscopy, which gives both structural and chemical information^[3,21].

Understanding how defects affect optical properties is a first essential step towards controlled functionalization of materials, both for fingerprinting (optical characterization is simple, remote, and non-destructive) and to understand derived optical functionalities. First-principles computational techniques provide a high degree of physical insight and predictive power in the spectral features of defects, to find new peaks and yield quantitative positions and weight transfers.

In this work, we present a fully First-principles investigation of defected monolayers of WS₂, based on the Bethe Salpeter Equation (BSE) for electron-hole interactions within many body perturbation theory. We analyze the resulting changes in electronic band structure and optical absorption spectra, aiming to answer the question: can we identify a defect, and ideally quantify its concentration^[22], just by looking at the absorption spectrum? While chalcogenide vacancies have been subject to some studies^[22], metal vacancies and isovalent substitutions like Mo_W and (CH₂)_S are still largely unreported, limiting our knowledge of their behaviour as quantum emitters or chemical detectors. We find that defects fall into two functional categories, based on the presence of bound states within the band-gap of WS₂. We discuss their spectra, spin textures and the criteria which could be used to identify each defect.

In **Figure 1** we show the four defects that are the focus of our work: two vacancies (S and W ions); and two substitutions, Mo_W and (CH₂)_S. The S vacancy is the most commonly found defect in monolayers of WS₂ and often assigned to specific features below the optical gap^[18]. In the substitution case Mo_W is quite commonly found in nature, and carbon is a common dopant in semiconductors^[23]. Studies have been made on the potential transport applications of TMDs and transition metal carbides^[13,24]. In the case of MoS₂ experiments point to changes to the electronic structure due to carbon doping, which should translate into new optical features^[15,25].

In ideal defect engineering, induced changes in the system should yield new controllable features that are distinct from the pristine properties. In the case of TMDs, a key property that relates to optics is the polarisation of states at the K wave vector in the Brillouin zone. The polarization will control the allowed optical transitions that form bright excitons. We label in order of increasing energy the last two occupied states and the first two unoccupied states at K as (v_1, v_2, c_1, c_2). For pristine WS₂ (see the Supplementary Material for more information), the first bright exciton would be made of an optical transition from v_2 to c_1 , while the second brightest exciton would be made by a transition from v_1 to c_2 . This is due to the fact that optical selection rules enforce spin conservation in TMDs: the valence and conduction manifold differ in orbital character, guaranteeing the needed angular momentum change when absorbing a helical photon^[26].

We start by analyzing two systems which feature states in the pristine band gap: the sulfur and tungsten vacancies. Their DFT band structures are shown in Figure 1 a) and 1 c), respectively. Note that using a 5×5 supercell, the point K of the pristine Brillouin zone (BZ) folds back into the point K of the supercell BZ.

Both systems preserve the spin polarisation of pristine states at K, meaning that the A and B peaks that are the dominant features of the pristine spectrum must also be present. For the S vacancy, Figure 1 a), new non-dispersive mid-gap singlet states appear 1.08 and 1.28 eV above the valence band edge, in agreement with what was previously found^[16,27]. At K the first band is almost completely spin-unpolarized, while the second is completely polarized. This opens a path for new emission channels, as electronic transitions from the pristine valence states to these new defect states are allowed, with different oscillator strengths and different excitation energies.

The W vacancy is more challenging numerically: the defect bands are split off from the bulk conduction and valence bands, but in the 5×5 supercell they still show some dispersion and a finite band width. Their position and spin texture are close to what has been found in other DFT calculations for this defect using larger supercells^[16], and we extract a semi-quantitative picture of the optical properties. Together with the six new mid-gap states, there are also four new occupied states bound to the defect

in the valence region (unlike the S vacancy). All these states are spin polarized at K, so if we consider optical selection rules, we can expect new peaks to show up in the absorption spectrum. These peaks will be a combination of transitions between pristine and defect states, and others between defect states (occupied to empty) in the mid-gap region.

The effects of changes in the band structure on the BSE optical spectrum are shown in **Figure 3**. For comparison the absorption spectrum of the pristine system is shown in grey. The energies of all identified excitons are listed in Table 1 in the SI, along with the reference energies for the pristine case. Note in passing that the higher energy peaks beyond A and B are not reproduced in full in our calculations, due to limitations in the number of states included in the BSE for such large systems.

With an S vacancy in Figure 1 a) two new peaks arise at 1.35 and 1.14 eV due to the mid-gap states. They are marked D₁ and D₂ in Figure 1 b). As shown in the inset, D₁ and D₂ correspond to optical transitions from the top valence band to the defect state at 1.28 eV and 1.08 eV, respectively. However, since the lowest defect state is not fully polarized, the resulting dipole matrix element is much smaller than that of the D₁ peak, where the defect state is fully polarized.

The exciton wave function for the peak corresponding to D₁ is shown in Figure 3 a). Here the hole is placed at the position of the vacant sulfur ion (marked by the green sphere) and the magnitude on the colour-map shows the probability density of the electron (see the Figure 5 in the SI where all the excitonic wave functions are depicted). The color map shows that exciton states are highly localized on the neighboring tungsten atoms, indicating that the S vacancy does indeed form a quantum dot.

For the W vacancy, whose spectrum is shown in Figure 1 d), more peaks are present due to the increased number of defect states. In total we identify five excitons: three composed from holes in the valence band and electrons in defect states, D₁ to D₃; and two others with both the electron and the hole bound to two different manifolds of defect states, D₄ and D₅. The states involved in the formation in the excitons are shown in the inset of Fig 1 d). The most striking feature is the relative intensity of the D₄ and D₅ excitons relative to the A and B excitons. As defect states have very weak dispersion, the associated electrons and holes will have large effective masses. It is possible to show^[28] that oscillator strengths are proportional to the reduced mass of electron and hole, which explains why the effect is further magnified for transitions *between* defect states in the case of the W vacancy.

A more detailed analysis to the excitonic wave functions shows that two of the low intensity peaks (D₁ and D₃) are artefacts due to the interaction of defect states in neighboring periodic replicas. They result from electron-hole pairs localized on different vacancy sites (see Figure 7 in the SI for zoomed out plots of excitonic wave function). The majority of the electronic charge in the exciton is not localized near the same ion vacancy as the hole, and is bound thanks to a finite overlap of the DFT defect state wave-functions. These two peaks will disappear if larger supercells are used: the dipole matrix element and oscillator strength will go to 0. We note that while the BSE is solved only for $\mathbf{q} = 0$, the introduction of non-dispersive defect states allows for many transitions to occur throughout the BZ, so an exciton function can actually be composed of several vertical transitions at different momenta (NB: this is distinct from a finite wave vector for the whole exciton).

In the case of D₂, shown in Figure 7 in the SI, there is a residual interaction with adjacent vacancy sites, but now the hole is correctly bound to an electron located at the same site. For D₅, shown in Figure 3 b) both the electron and hole are entirely located at the same site.

We studied two cases of substitutions in the WS₂ monolayer; one with a molybdenum atom replacing a tungsten atom; and another where a sulfur atom was replaced by a methyl, the simplest (divalent) group representing grafted organic substituents.

In both cases no mid gap states were found (see Figure 4 in the SI for their bandstructures), which can be rationalized as follows. In the case of Mo_W substitution, molybdenum and tungsten have the same valence, close atomic and covalent radii^[29–31], resulting in similar chemical properties. A small concentration of defects does not lead to strong changes in the charge density, thus leaving the system practically unchanged when compared to the pristine case. For the (CH₂)_S substitution, the methylene group provides the same number of valence electrons as the sulfur atom. The breaking of local symmetry is not strong enough to perturb the band edges.

The lack of mid-gap states is reflected in the absorption spectra shown in **Figure 4**. In both cases the excitonic peaks lie almost on top of those of the pristine system, with the largest deviation being 60 meV for the Mo_W A peak. The energies for the defected A and B peaks are shown in Table 1 in the SI. There is, however, both weight transfer and changes in spin texture for the A and B peaks at higher energies in the absorption spectrum of both substitutions, which suggests methods to identify these defects experimentally. The strongest signature of the substitution lies within the exciton wave functions shown in **Figure 5**. While the exciton cloud is still dispersed throughout the crystal, there is a higher charge concentration near the substitution. In the (CH₂)_S case this is valid for the A exciton (Figure 5 c)), and in Mo_W both A and B excitonic states localize near the defect. The (CH₂)_S case also shows breaking of C₃ symmetry by the methyl molecule. The localization is due both to the defect-related electronic states and to the choice of the initial position of the hole. For reference, in boron nitride similar extensions of 3-5 nearest neighbors are found in Ref.^[32].

The two peaks which correspond to the bulk excitons A and B known from literature, and are within 50 meV of those of the pristine system in all cases (this is below the absolute precision of the first principles methods, and shows the basic convergence of our supercell sizes).

We can now establish a more complete picture of how different defects change optical properties of TMDs. The main changes to the optical spectrum come from new mid-gap states. Isovalent substitutions like Mo_W and (CH₂)_S will not be trivially seen in the absorption spectra, but can still be detected by the ratio of the A and B peak intensities, and by localisation in the exciton’s spatial distribution.

In terms of potential applications, the two vacancies are clear front runners for designing quantum dots and quantum emitters. In particular the S vacancy has already shown some promising results as a single photon emitter^[33]. The two mid-gap defect states are actively considered for quantum computing applications: they are separated in energy by 0.21 eV, making them addressable using mid-infrared lasers, and insulating them from the highest phonon energy in pristine WS₂, which is 53 meV^[34,35].

The W vacancy offers a larger set of localized excitons, but is more energetic and harder to produce (see Table 1 in the SI). Here the brightest excitons are made of transitions between single particle defect states, due to their large effective masses. These exciton states show potential in devices as they would behave as bright emitters with multiple internal states, behaving like an embedded molecule for multi-valued quantum computing^[36]. The residual band width will disappear only in a 7×7 supercell^[16], but the spin texture and qualitative features are already well represented here (see Figure 3 in the SI). In actual samples, this vacancy type is more likely to be charged, with electrons filling the dangling S ion’s orbitals.

We have shown that the isovalent substitutions Mo_W and (CH₂)_S will not produce in-gap states. Though this is intuitive, it is not trivial, and the local electronic structure is strongly modified as shown by the excitonic wave functions. For purposes of grafting organic molecules, this means the full band gap window of intrinsic WS₂ will be available for optical sensing.

In conclusion, we employ powerful and accurate first principles techniques to shed some light into the changes in optical properties introduced by point defects in TMDs. Two promising systems, S and W ion vacancies, have potential for quantum emitters and even quantum computing. Isovalent vacancies do not introduce mid-gap states in the band structure, but do change the relative intensity of the canonical A and B peaks, and the spatial distribution of the first and second excitonic states, in the (CH₂)_S case even leading to a breaking of symmetry. In both cases the full sub optical gap region is available for use in detection of molecules that might graft themselves onto the TMD’s surface.

Supporting Information

Supporting Information is available from the Wiley Online Library. Additional details on the convergence with cell size, the wave functions for all defect-bound exciton states, and DFT and Many-body Perturbation theory methods and numerical parameters used in our calculations.

Acknowledgements

We wish to acknowledge important input, discussions, and stimulus from M. Terrones, B. Biel, and M. Palummo, as well as extensive support from the Yambo developer team.

PMMCM and MJV acknowledge funding by the Belgian FNRS (PDR G.A. T.1077.15, T.0103.19, and an “out” sabbatical grant to ICN2 Barcelona), and the Communauté Française de Belgique (ARC AIMED G.A. 15/19-09). This publication is based upon work of the MELODICA project, funded by the EU FLAG-ERA_JTC2017 call.

The work benefited from HPC-EUROPA3 (INFRAIA-2016-1-730897) H2020 Research Innovation Action hosted by the Theory and Simulation group at ICN2 supported by the Barcelona Supercomputing Center, and from the access provided by ICN2 (Barcelona, Spain) within the framework of the NFFA-Europe Transnational Access Activity (grant agreement No 654360, proposal ID 717, submitted by PMMCM).

Z.Z. acknowledges support by the Ramón y Cajal program RYC-2016-19344 (MINECO/AEI/FSE, UE), Spanish MINECO (FIS2015-64886-C5-3-P), the Severo Ochoa Program (MINECO, SEV-2017-0706), the CERCA programme of the Generalitat de Catalunya (Grant 2017SGR1506), the EC H2020-INFRAEDI-2018-2020 MaX Materials Design at the Exascale CoE (grant No. 824143), and the Netherlands sector plan program 2019-2023.

Computational resources have been provided by the Consortium des Equipements de Calcul Intensif (CECI), funded by FRS-FNRS G.A. 2.5020.11; the Zenobe Tier-1 supercomputer funded by Walloon G.A. 1117545; and by PRACE DECI grants 2DSpin and Pylight on Beskow (G.A. 653838 of H2020, and FP7 RI-312763). The authors thankfully acknowledge the computer resources at Mare Nostrum technical support provided by the Barcelona Supercomputing Center (Spanish Supercomputing Network, RES). This publication is based upon work from COST Action TUMIEE (CA17126), supported by COST (European Cooperation in Science and Technology).

Conflicts of Interest

The authors have no commercial or financial conflicts of interest.

References

- [1] Q. H. Wang, K. Kalantar-Zadeh, A. Kis, J. N. Coleman, M. S. Strano, *Nature Nanotechnology* **2012**, *7*, 11 699.
- [2] K. F. Mak, J. Shan, *Nature Photonics* **2016**, *10*, 4 216.
- [3] D. Edelberg, D. Rhodes, A. Kerelsky, B. Kim, J. Wang, A. Zangiabadi, C. Kim, A. Abhinandan, J. Ardelean, M. Scully, D. Scullion, L. Embon, R. Zu, E. J. G. Santos, L. Balicas, C. Marianetti, K. Barmak, X. Zhu, J. Hone, A. N. Pasupathy, *Nano Letters* **2019**, *19*, 7 4371.
- [4] N. Briggs, S. Subramanian, Z. Lin, X. Li, X. Zhang, K. Zhang, K. Xiao, D. Geohegan, R. Wallace, L.-Q. Chen, M. Terrones, A. Ebrahimi, S. Das, J. Redwing, C. Hinkle, K. Momeni, A. van Duin, V. Crespi, S. Kar, J. A. Robinson, *2D Materials* **2019**, *6*, 2 022001.
- [5] H.-P. Komsa, J. Kotakoski, S. Kurasch, O. Lehtinen, U. Kaiser, A. V. Krasheninnikov, *Physical Review Letters* **2012**, *109*, 3 035503.
- [6] S. Feng, Z. Lin, X. Gan, R. Lv, M. Terrones, *Nanoscale Horizons* **2017**, *2*, 2 72.
- [7] Z. Lin, B. R. Carvalho, E. Kahn, R. Lv, R. Rao, H. Terrones, M. A. Pimenta, M. Terrones, *2D Materials* **2016**, *3*, 2 022002.
- [8] R. Bourrellier, S. Meuret, A. Tararan, O. Stéphan, M. Kociak, L. H. Tizei, A. Zobelli, *Nano Letters* **2016**, *16*, 7 4317.
- [9] M. Ersfeld, F. Volmer, P. M. M. C. de Melo, R. de Winter, M. Heithoff, Z. Zanolli, C. Stampfer, M. J. Verstraete, B. Beschoten, *Nano Letters* **2019**, *19*, 6 4083.
- [10] A. Bolotsky, D. Butler, C. Dong, K. Gerace, N. R. Glavin, C. Muratore, J. A. Robinson, A. Ebrahimi, *ACS Nano* **2019**, *13*, 9 9781.

- [11] J. Azadmanjiri, P. Kumar, V. K. Srivastava, Z. Sofer, *ACS Applied Nano Materials* **2020**, *3*, 4 3116.
- [12] L. W. Yang, P. D. Wright, V. Eu, Z. H. Lu, A. Majerfeld, *Journal of Applied Physics* **1992**, *72*, 5 2063.
- [13] Z. Hai, J. Du, M. K. Akbari, C. Xue, H. Xu, S. Zhuiykov, *Ionics* **2017**, *23*, 7 1921.
- [14] J. Wu, L. Ma, A. Samanta, M. Liu, B. Li, Y. Yang, J. Yuan, J. Zhang, Y. Gong, J. Lou, R. Vajtai, B. Yakobson, A. K. Singh, C. S. Tiwary, P. M. Ajayan, *Advanced Materials Interfaces* **2017**, *4*, 4 1600866.
- [15] Q. Yue, S. Chang, S. Qin, J. Li, *Physics Letters A* **2013**, *377*, 19 1362.
- [16] M. A. Khan, M. Erementchouk, J. Hendrickson, M. N. Leuenberger, *Phys. Rev. B* **2017**, *95*, 24 245435.
- [17] B. Schuler, J.-H. Lee, C. Kastl, K. A. Cochrane, C. T. Chen, S. Refaely-Abramson, S. Yuan, E. van Veen, R. Roldán, N. J. Borys, R. J. Koch, S. Aloni, A. M. Schwartzberg, D. F. Ogletree, J. B. Neaton, A. Weber-Bargioni, *ACS Nano* **2019**, *13*, 9 10520.
- [18] V. Carozo, Y. Wang, K. Fujisawa, B. R. Carvalho, A. McCreary, S. Feng, Z. Lin, C. Zhou, N. Perea-López, A. L. Elías, B. Kabius, V. H. Crespi, M. Terrones, *Science Advances* **2017**, *3*, 4 e1602813.
- [19] T. Y. Jeong, H. Kim, S.-J. Choi, K. Watanabe, T. Taniguchi, K. J. Yee, Y.-S. Kim, S. Jung, *Nature Communications* **2019**, *10*, 1 3825.
- [20] J. Dang, S. Sun, X. Xie, Y. Yu, K. Peng, C. Qian, S. Wu, F. Song, J. Yang, S. Xiao, L. Yang, Y. Wang, M. A. Rafiq, C. Wang, X. Xu, *npj 2D Materials and Applications* **2020**, *4*, 1 2.
- [21] J. Hong, R. Senga, T. Pichler, K. Suenaga, *Physical Review Letters* **2020**, *124*, 8 87401.
- [22] S. Refaely-Abramson, D. Y. Qiu, S. G. Louie, J. B. Neaton, *Physical Review Letters* **2018**, *121*, 16 167402.
- [23] Y. J. Zheng, Y. Chen, Y. L. Huang, P. K. Gogoi, M.-Y. Li, L.-J. Li, P. E. Trevisanutto, Q. Wang, S. J. Pennycook, A. T. S. Wee, S. Y. Quek, *ACS Nano* **2019**, *13*, 5 6050.
- [24] J. Jeon, Y. Park, S. Choi, J. Lee, S. S. Lim, B. H. Lee, Y. J. Song, J. H. Cho, Y. H. Jang, S. Lee, *ACS Nano* **2018**, *12*, 1 338.
- [25] A.-M. Hu, L.-l. Wang, W.-Z. Xiao, G. Xiao, Q.-Y. Rong, *Computational Materials Science* **2015**, *107* 72.
- [26] A. Molina-Sánchez, D. Sangalli, L. Wirtz, A. Marini, *Nano Letters* **2017**, *17*, 8 4549.
- [27] B. Schuler, D. Y. Qiu, S. Refaely-Abramson, C. Kastl, C. T. Chen, S. Barja, R. J. Koch, D. F. Ogletree, S. Aloni, A. M. Schwartzberg, J. B. Neaton, S. G. Louie, A. Weber-Bargioni, *Physical Review Letters* **2019**, *123*, 7 76801.
- [28] C. Hamaguchi, *Basic Semiconductor Physics*, Graduate Texts in Physics. Springer International Publishing, Cham, **2017**.
- [29] B. Cordero, V. Gómez, A. E. Platero-Prats, M. Revés, J. Echeverría, E. Cremades, F. Barragán, S. Alvarez, *Dalton Transactions* **2008**, , 21 2832.
- [30] P. Pyykkö, M. Atsumi, *Chemistry - A European Journal* **2009**, *15*, 46 12770.
- [31] P. Pyykkö, M. Atsumi, *Chemistry - A European Journal* **2009**, *15*, 1 186.
- [32] F. Paleari, T. Galvani, H. Amara, F. Ducastelle, A. Molina-Sánchez, L. Wirtz, *2D Materials* **2018**, *5*, 4 45017.

- [33] Y. M. He, G. Clark, J. R. Schaibley, Y. He, M. C. Chen, Y. J. Wei, X. Ding, Q. Zhang, W. Yao, X. Xu, C. Y. Lu, J. W. Pan, *Nature Nanotechnology* **2015**, *10*, 6 497.
- [34] N. A. Pike, A. Dewandre, B. Van Troeye, X. Gonze, M. J. Verstraete, *Physical Review Materials* **2018**, *2*, 6 63608.
- [35] N. A. Pike, A. Dewandre, B. Van Troeye, X. Gonze, M. J. Verstraete, *Physical Review Materials* **2019**, *3*, 7 74009.
- [36] B. Fresch, M. V. Klymenko, R. D. Levine, F. Remacle, 295–318. Springer International Publishing, Cham, ISBN 978-3-319-65826-1, **2018**, URL https://doi.org/10.1007/978-3-319-65826-1_{_}15.

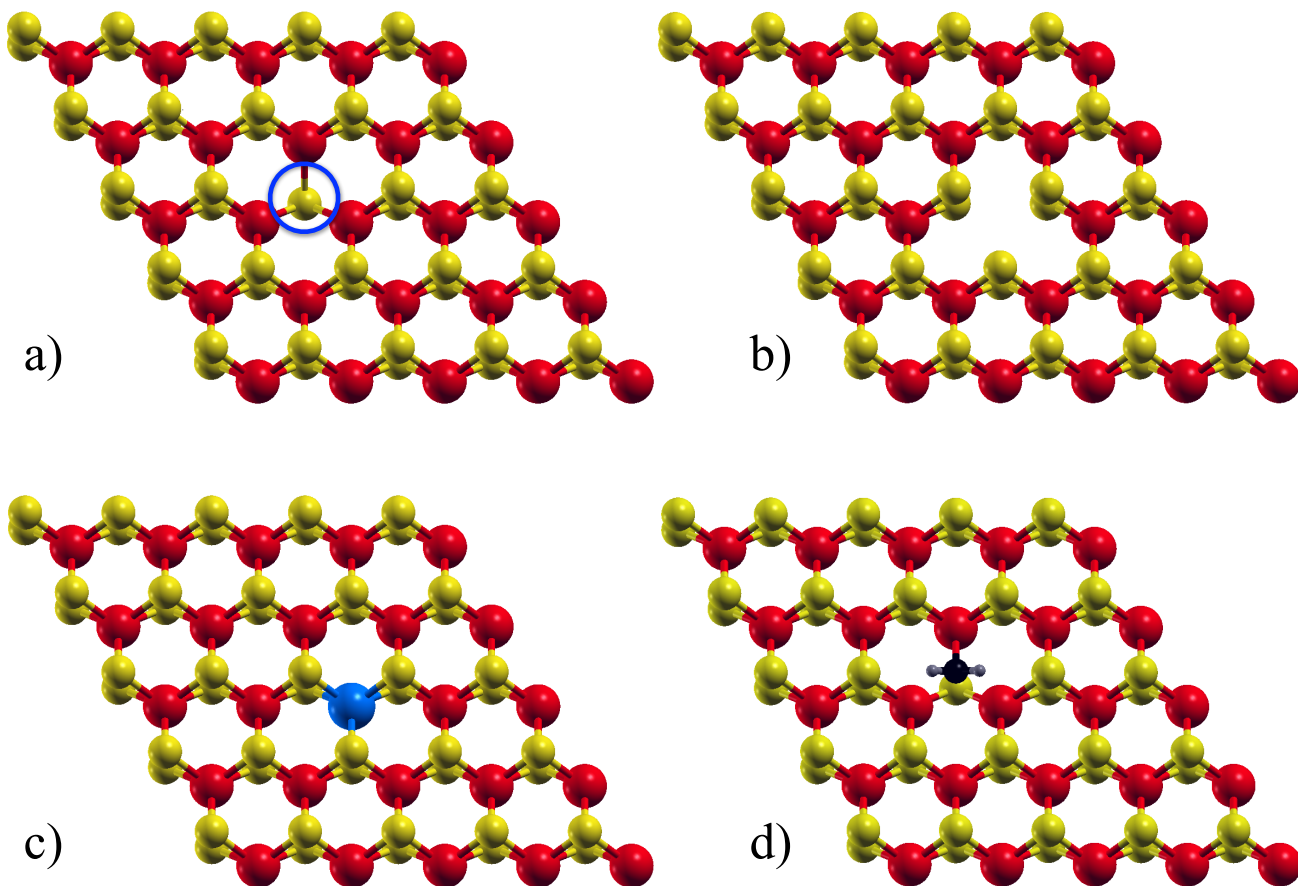


Figure 1: Defected 5×5 supercells used in this work. a) S vacancy, marked by the blue circle. b) W vacancy. c) MoW substitution. d) $(\text{CH}_2)_\text{S}$ substitution. Tungsten atoms are shown in red, sulfur in yellow, molybdenum in blue, carbon in black, and hydrogen in grey.

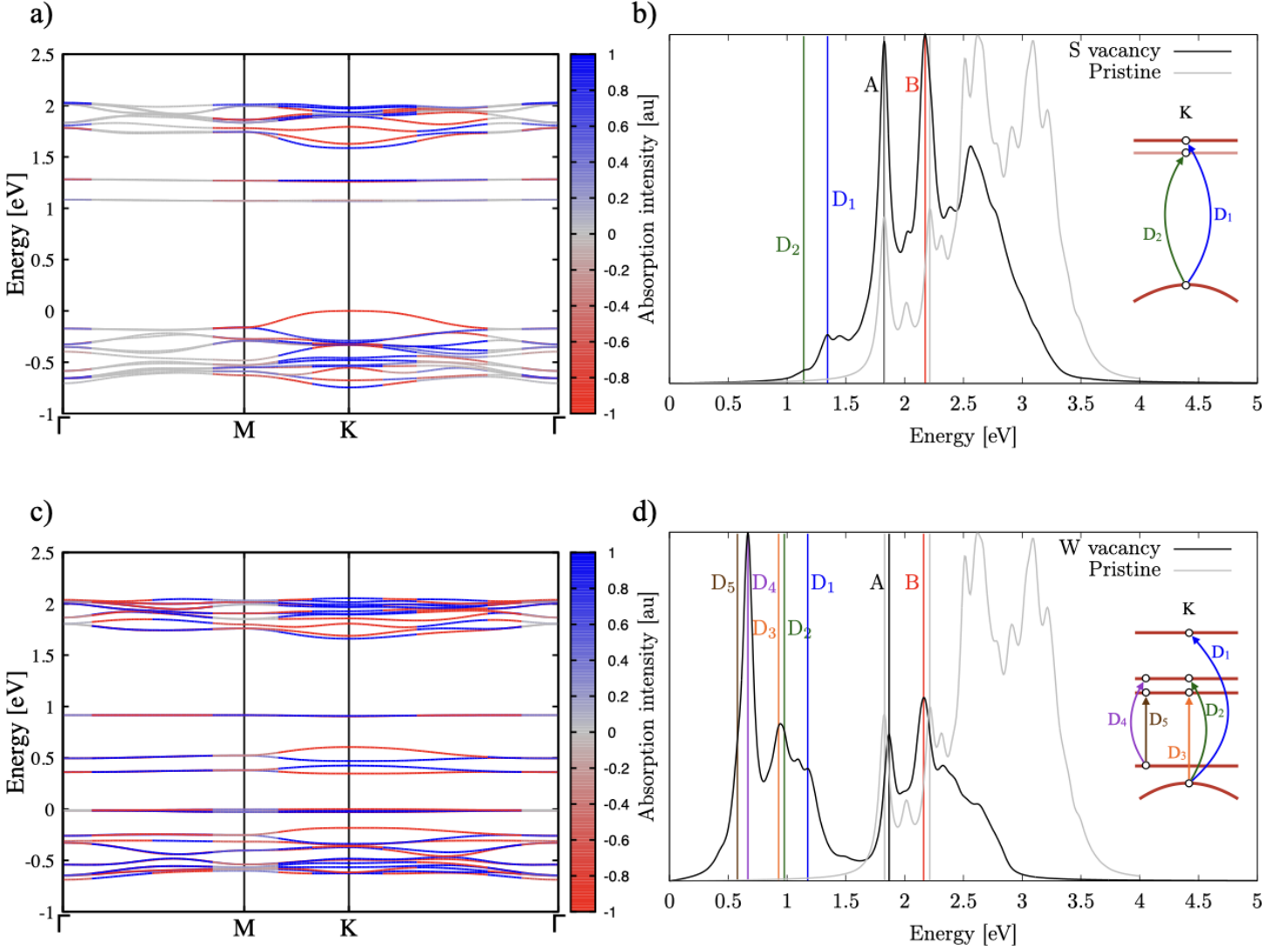


Figure 2: (color online) a) and c): DFT band structures and spin-texture of defected WS₂ for the S and W vacancies, respectively. Color scale indicates value of $\langle S_z \rangle$ (red for 1 and blue for -1). The reference Fermi level at 0 is set to the last occupied state. In both cases new states arise in the mid-gap region, with new occupied defect states also showing in the W vacancy's band structure. b) and d): Optical absorption spectra of the S and W vacancies, respectively. Absorption of the pristine system is shown in grey. The positions of the first excitonic peaks are shown by vertical lines. Labels and vertical lines have matching colours. Two new peaks arise for the S vacancy due to the two new manifolds of mid-gap states. The W vacancy exhibits several new peaks, as four new manifolds of defect states arise. The insets in b and d show the level scheme and main excitonic transitions.

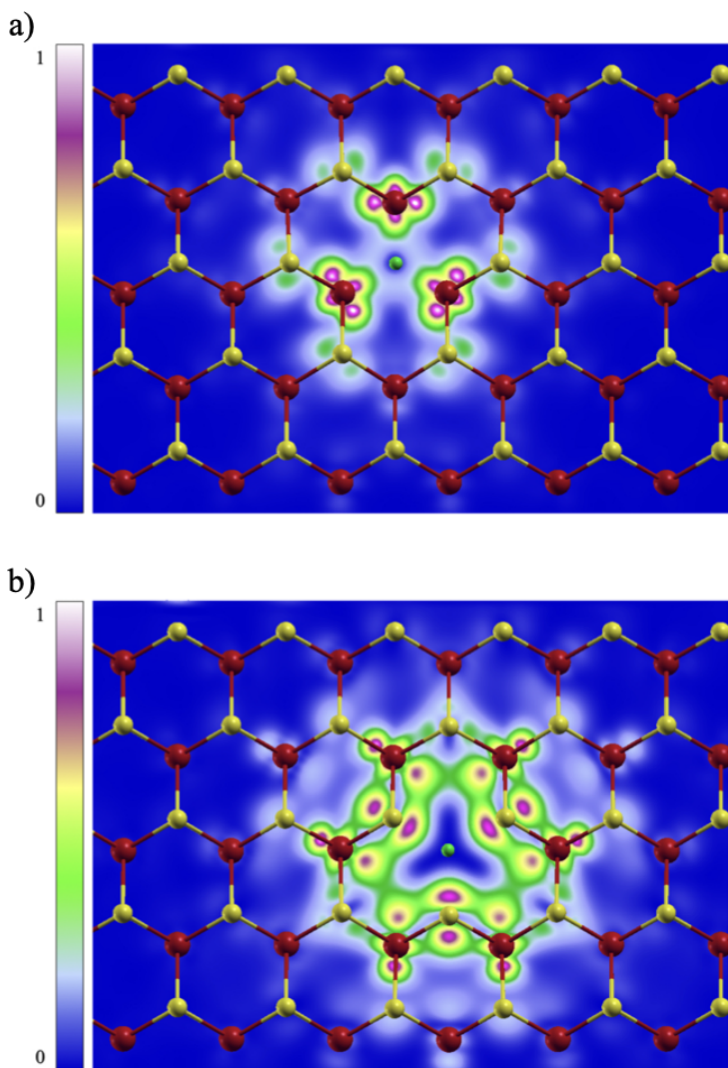


Figure 3: (color online) a) S vacancy wave function for excitonic state D_2 , shown in Figure 1 b). b) W vacancy wave function for excitonic state D_5 , shown in Figure 1 d). The hole is marked by the green sphere and it is placed at the position of the missing sulfur ion. In both cases the electronic charge is highly localized near the hole, indicating the formation of a quantum dot.

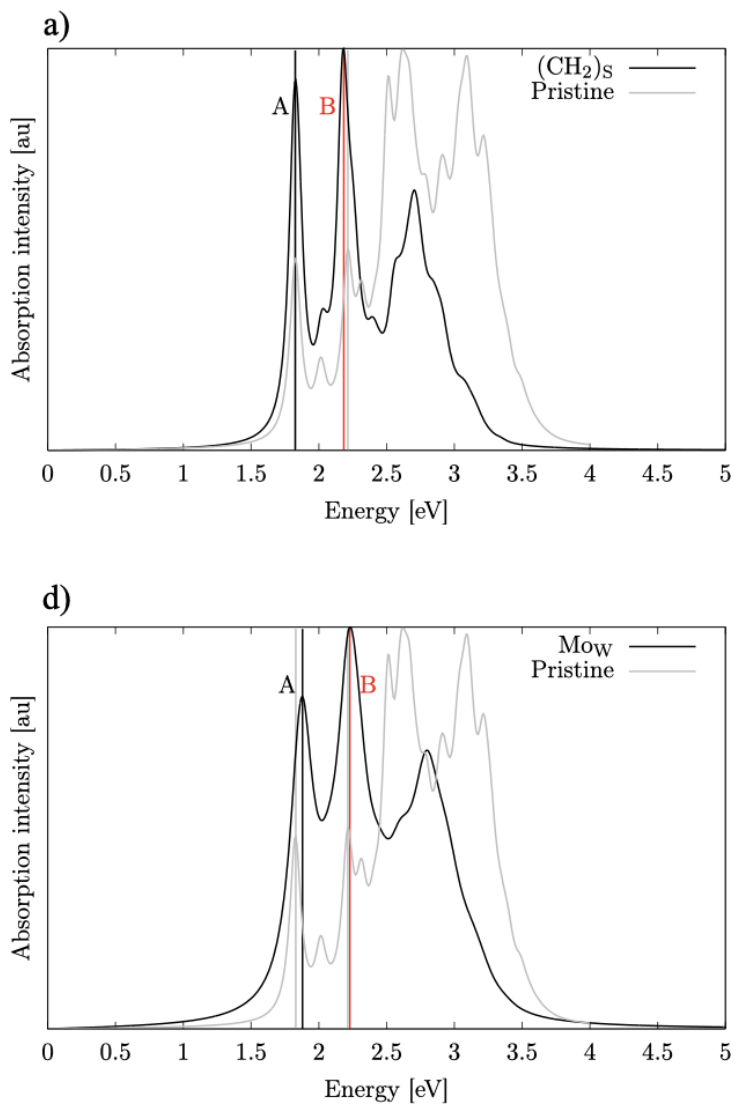


Figure 4: (color online) Optical absorption spectra for the 5×5 supercells with the a) Mo_W substitution; b) $(\text{CH}_2)_S$ substitution. Absorption of the pristine system is shown in grey. The positions of the first excitonic peaks are shown by vertical lines. Labels and vertical lines have matching colours. Both cases show no new peaks, with the A and B excitons at energies that almost match those of the pristine case.

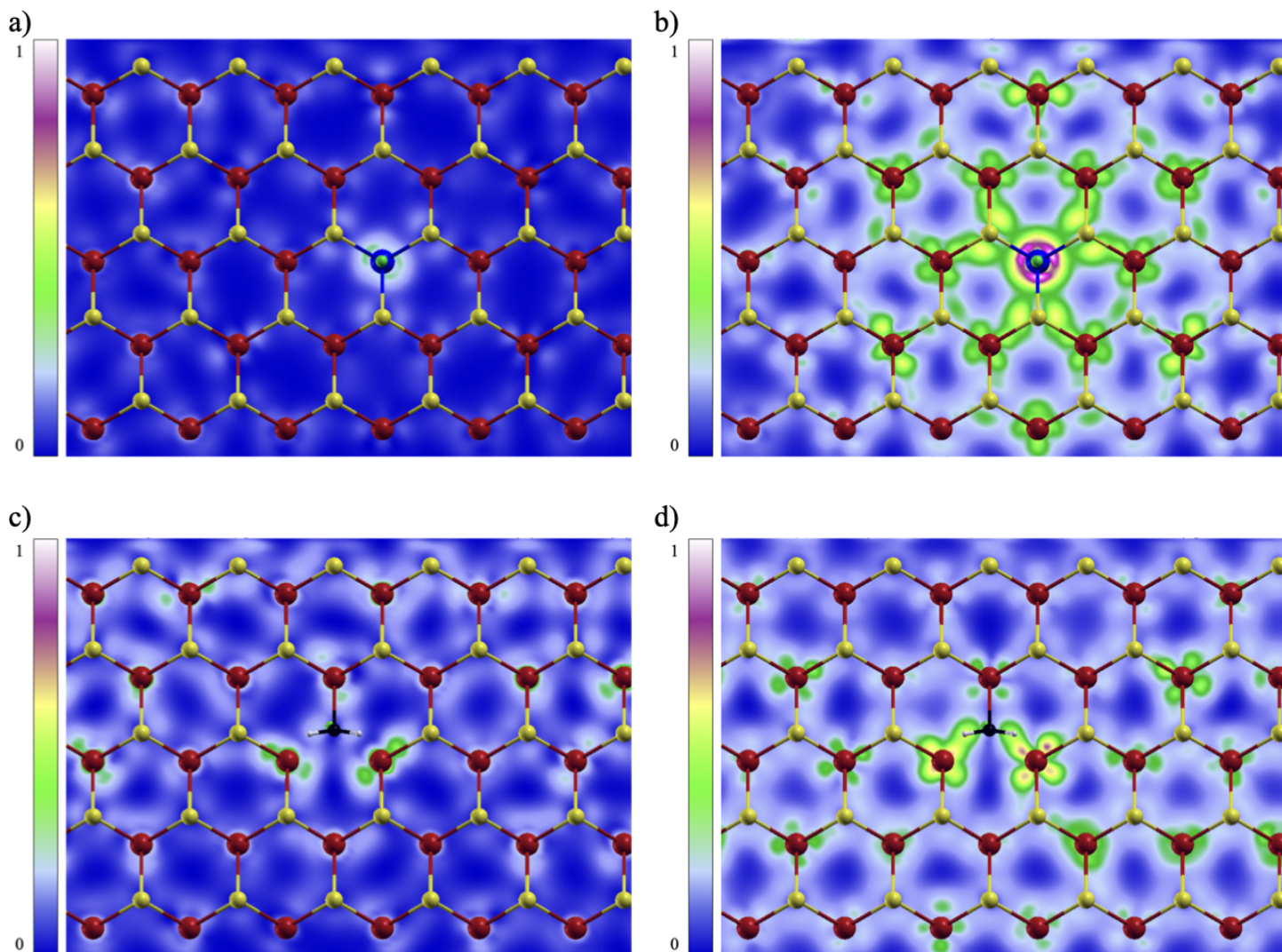
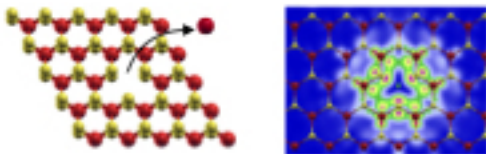


Figure 5: A (left column) and B (right) excitonic wave functions of MoW (a) and b)) and $(\text{CH}_2)_\text{S}$ (c) and d)), shown in Figure 4. The hole is marked by the green sphere and it is placed between the the mid-plane and the carbon ion. While there is some charge localisation and symmetry breaking, the exciton wave function extends through the whole system.

Table of Contents



Large and defectless monolayers of transition metal dichalcogenides (TMDs) are difficult to manufacture, with most of them containing defects. Herein it is shown using Many-Body Perturbation Theory how different vacancies and substitutions can in fact be advantageous, by creating new quantum dots or adsorption sites in the monolayer, thus increasing its functionalization potential.